Green Chemistry

PAPER

View Article Online
View Journal | View Issue

Cite this: *Green Chem.*, 2024, **26**, 2605

Benzotrifuran-based donor–acceptor covalent organic frameworks for enhanced photocatalytic hydrogen generation†

Chuanmeng Yang,‡[a] Zhenwei Zhang,‡[a] Jiali Li,[a] Yuxin Hou,[a] Qi Zhang,*[b] Zhongping Li,[d] Huijuan Yue[c] and Xiaoming Liu*[a]

Visible-light-driven hydrogen evolution from water represents a green and sustainable technology to convert solar energy into chemical energy. Covalent organic frameworks (COFs) are the most competitive platforms among the variety of photocatalysts. Herein, a novel benzotrifuran-based donor–acceptor material (COF-JLU42) was constructed using a Schiff base polycondensation reaction by introducing electron-rich benzotrifuran and deficient triazine moieties into the framework. The new COF features high crystallinity and permanent porosity with a large surface area and proves to be a photoactive semiconductor with efficient visible-light harvesting capacity. Importantly, COF-JLU42 exhibits a superior photocatalytic activity with a hydrogen evolution rate of over 40 000 μmol g^{-1} h^{-1} under visible-light illumination, which is 2.5 times higher than that of the isomorphic benzotrithiophene-based COFs under the same conditions. These findings suggest the huge application prospect of benzotrifuran-based framework materials as metal-free and solid photocatalysts in solar-energy conversion and storage.

Received 15th December 2023,
Accepted 18th January 2024

DOI: 10.1039/d3gc04972h

rsc.li/greenchem

Introduction

Sunlight-driven photocatalytic hydrogen production from water is a green and sustainable technology for the conversion of solar energy into chemical energy to alleviate the serious energy crisis and environmental pollution problems.[1–4] Semiconductor photocatalysts are the key aspect in the whole catalytic process because they are responsible for visible-light harvesting, charge carrier transport and separation, as well as surface redox reactions.[5] Therefore, over the past decades, great efforts have been devoted to constructing highly effective semiconductor photocatalysts, including inorganic metal oxides[6,7] and organic polymers such as graphite carbon nitride (g-C_3N_4),[8–13] to realize sustainable light-driven hydrogen evolution. However, inefficient visible-light absorption, expensive metals, and rapid charge recombination seriously hinder their practical applications.[8]

Covalent organic frameworks (COFs) have emerged as a new class of porous crystalline polymers by integrating functional organic building units into periodic network architectures through strong covalent bonds under reticular chemistry.[12–18] Considering structural aspects, their inherent ordered pores and large specific surface areas can provide large spaces for matter diffusion and transformation. Two-dimensional (2D) COFs offer columnar π-arrays and afford an ideal channel for photoinduced charge carrier transmission owing to the orbital overlap of stacked aromatic blocks.[17–23] As desirable alternatives to inorganic photocatalysts, metal-free 2D-COFs have recently received much attention in various heterogeneous photocatalysis, including photocatalytic hydrogen production.[24–34] In particular, the most important advantage of 2D-COFs is that it is easy to regulate their structure and functionality by selecting special building blocks as co-monomers and different linkages. For example, Lotsch *et al.* were the first to utilize a hydrazone-linked triazine-based COF[26] for photocatalytic hydrogen evolution under visible-light illumination. In 2018, Cooper and co-workers successfully prepared a fused-sulfone-based COF,[25] which provided a superior hydrogen evolution rate (HER) of 16.3 mmol g^{-1} h^{-1} when dye-sensitized. Subsequently, highly crystalline covalent triazine frameworks (CTFs)[25–37] and keto-enamine-like 2D-COFs[38,39] were

[a]*College of Chemistry, Jilin University, Changchun, 130012, P.R. China. E-mail: xm_liu@jlu.edu.cn*
[b]*School of Engineering, University of Warwick, Coventry CV4 7AL, UK. E-mail: 1033012429@qq.com*
[c]*State Key Laboratory of Inorganic Synthesis and Preparative Chemistry, College of Chemistry, Jilin University, Changchun 130012, P.R. China*
[d]*School of Energy and Chemical Engineering/Center for Dimension-Controllable Organic Frameworks, Ulsan National Institute of Science and Technology (UNIST), Ulsan, 44919, Republic of Korea*

†Electronic supplementary information (ESI) available: Synthetic procedures, full characterisation and spectroscopic data. See DOI: https://doi.org/10.1039/d3gc04972h

‡These authors contributed equally to manuscript.

proven to have outstanding hydrogen production performances with high photocatalytic activity. In addition, a series of functional organic building units such as triazine, pyrene, porphyrin, and phthalocyanine has been introduced into the frameworks to functionalise them.[17,18,21] However, designing and synthesizing novel organic structures as monomers to construct metal-free, high-performance COF-based photocatalysts with small exciton binding energy (E_b) and high photocatalytic activity are still highly desired.

It is well known that benzodifuran compounds with electron-rich properties are widely utilized as hole-transfer materials in organic light-emitting diodes and photovoltaic cells.[40,41] Recently, a few COFs containing benzodifuran moiety have emerged and demonstrated excellent photocatalytic properties.[42,43] Benzo[1,2-*b*:3,4-*b*′:5,6-*b*″]trifuran is a fused trifuran with an oxygen-rich, C_{3h} symmetry, planar and extended π-system, which has not been explored in the field of organic porous polymers.[17,18,21,44] In this context, we have successfully constructed a novel benzotrifuran-based COF material (named COF-JLU42) with an electron donor–acceptor (DA) character for photocatalytic hydrogen evolution *via* water splitting. Due to its high crystallinity, large porosity, and inherent built-in electric field with small E_b, COF-JLU42 showcases a superior photocatalytic activity with hydrogen evolution rate (HER) of 40 430 μmol g^{-1} h^{-1} under visible-light illumination, which is 2.5 times higher than that of the isomorphic benzotrithiophene-based COF under the same conditions.

Results and discussion

A novel benzotrifuran-based imine-linked DA framework material COF-JLU42 was synthesized by the condensation of benzo[1,2-*b*:3,4-*b*′:5,6-*b*″]trifuran-2,5,8-tricarbaldehyde (BTF-TC) as an electron donor and 2,4,6-tris(4-aminophenyl)-1,3,5-triazine (TAPT) as an electron acceptor in *o*-dichlorobenzene (*o*-DCB), 1-butanol and acetic acid (AcOH, 6 M) at 120 °C for 72 h (Fig. 1, for details see the ESI†), which produced a yellow powder at 90% yield. In order to compare the structure

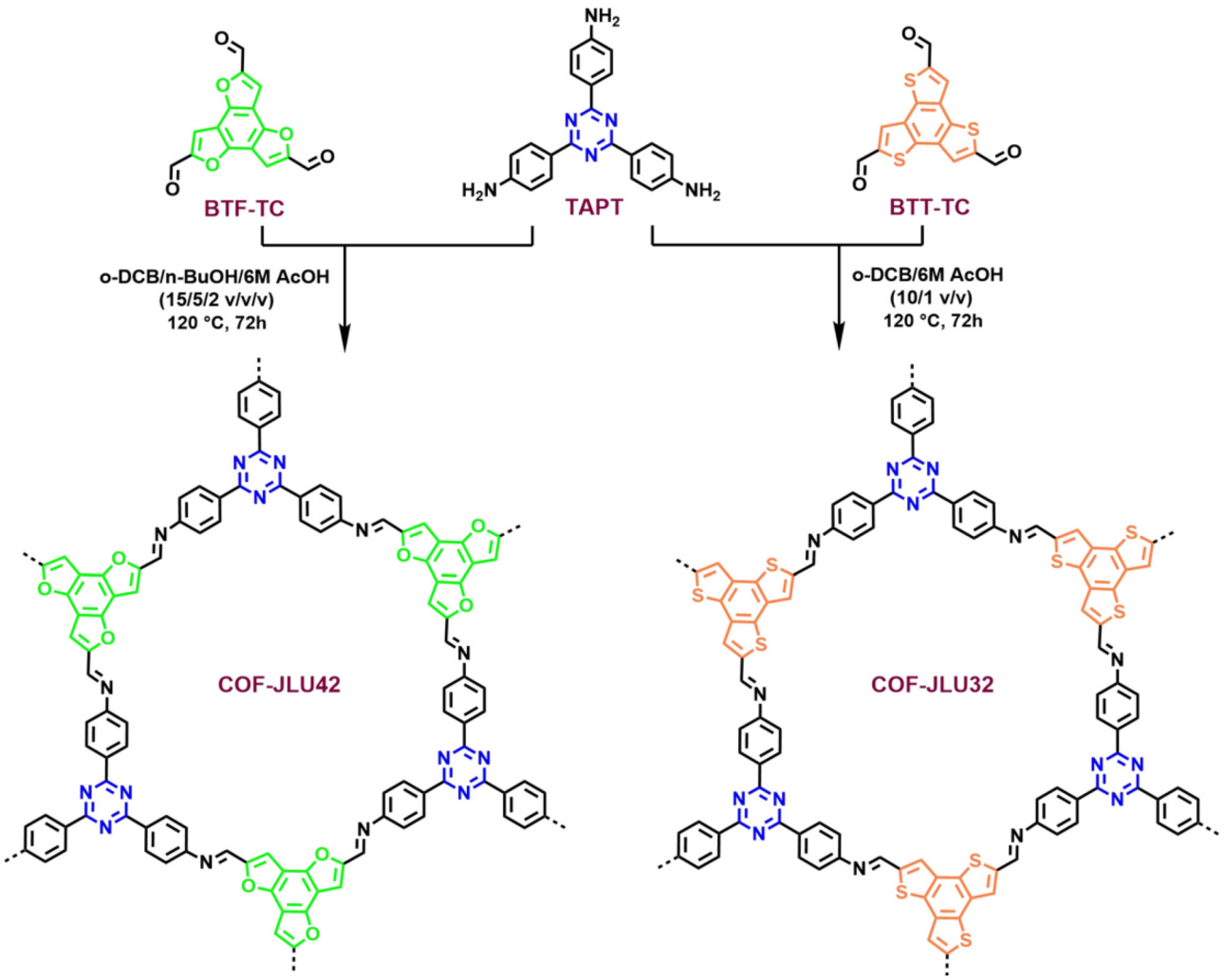

Fig. 1 Synthetic conditions and chemical structures of COF-JLU42 and COF-JLU32.

and properties, an isomorphic benzotrithiophene-based COF (COF-JLU32) was also synthesized according to the previously reported process (Fig. 1).[20] The COF-JLU42 was confirmed by Fourier transform infrared (FT-IR) spectroscopy and solid-state ^{13}C cross-polarization magic angle spinning (CP/MAS) NMR spectroscopy. Compared with the monomer BTF-TC, the characteristic vibration peak at 1686 cm^{-1} almost disappeared in the FT-IR spectrum of COF-JLU42. A strong stretching signal at 1626 cm^{-1} originating from the C=N group for COF-JLU42 was obtained, proving the formation of imine linkage (Fig. 2a). Furthermore, the chemical structure of COF-JLU42 at the molecular level was also researched by ^{13}C CP/MAS NMR analysis. As shown in Fig. 2b, the low-field signal at 167.2 ppm can be assigned to the carbon atom of the triazine ring. The peak at about 147.7 ppm is attributed to the imine group. In addition, other signals at 152.3, 133.2, 128.1, 116.4, 109.8, and 103.8 ppm are ascribed to the carbons in the aromatic rings. Those findings matched the carbon species in the structure of COF-JLU42.

The permanent porosity of COF-JLU42 was evaluated by utilizing the nitrogen (N_2) sorption isotherms at 77 K. As shown in Fig. 3a, the sorption curve of COF-JLU42 exhibited a typical type I reversible isotherm featured by a rapid N_2 uptake under a low relative pressure at $p/p_0 < 0.05$, which is a characteristic of microporous materials. Based on the adsorption curve, the Brunauer–Emmett–Teller (BET) surface area of COF-JLU42 was calculated to be 1375 $m^2\ g^{-1}$, which is smaller than that of isomorphic COF-JLU32 (1501 $m^2\ g^{-1}$).[20] The pore volume was 0.817 $cm^3\ g^{-1}$ at $p/p_0 = 0.99$. In addition, the nonlocal density functional theory (NLDFT) model indicated that the pore size distribution was concentrated at approximately 1.85 nm (Fig. 3b), which is reasonably close to its theoretical value of 1.9 nm.

The crystal structure of COF-JLU42 was investigated using powder X-ray diffraction (PXRD) analysis coupled with the Materials Studio simulations. The experimental PXRD pattern presents a strong peak at about 4.80°, and other relatively

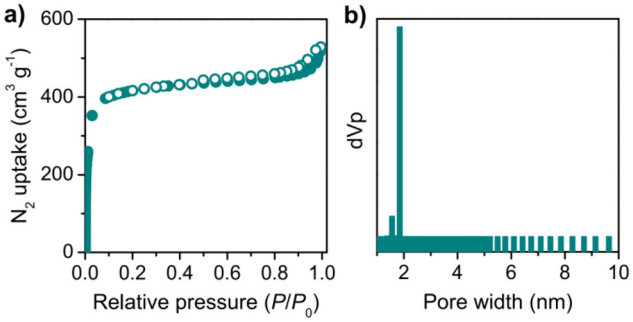

Fig. 3 (a) Nitrogen adsorption–desorption isotherm of COF-JLU42 measured at 77 K (adsorption: filled circle; desorption: open circle). (b) Pore size distribution of COF-JLU42.

weak signals at 8.28°, 9.76°, 12.7°, and 26.1°, which are assignable to the (100), (200), (210), (220), and (001) reflections of the hexagonal lattice (Fig. 4a, yellow line), respectively. The full width at half maximum (FWHM) of the peak at $2\theta = 1.80°$ for COF-JLU42 was calculated as 0.46° (Fig. S1a†), which is larger than that of COF-JLU32 (0.37°, Fig. S1b†), implying that COF-JLU42 has slightly weaker crystallinity than the latter.[20] The theoretical simulation of the crystal structure demonstrated that the COF-JLU42 tended to stack in the AA model (Fig. 4a, green line). Pawley refinement showed that the XRD curve was coincident with the obtained pattern, as evidence of negligible distinction (Fig. 4a, yellow-green line; R_p = 5.85% and R_{wp} = 7.85%). In addition, field-emission scanning elec-

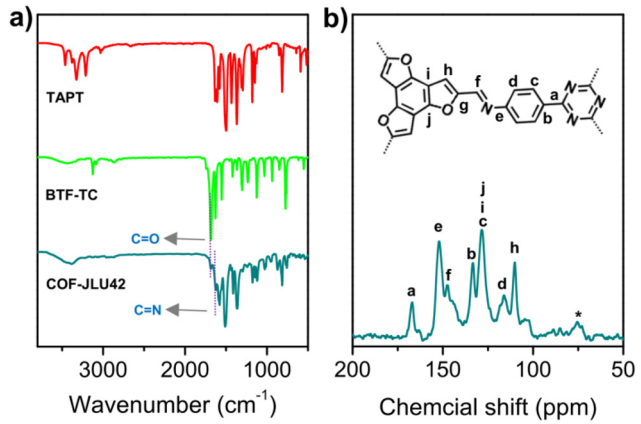

Fig. 2 (a) FT-IR spectra of COF-JLU42 and corresponding monomers. (b) Solid-state ^{13}C spectra of COF-JLU42, inset: the chemical structure of COF-JLU42. Asterisk (*) indicates a peak arising from a spinning band.

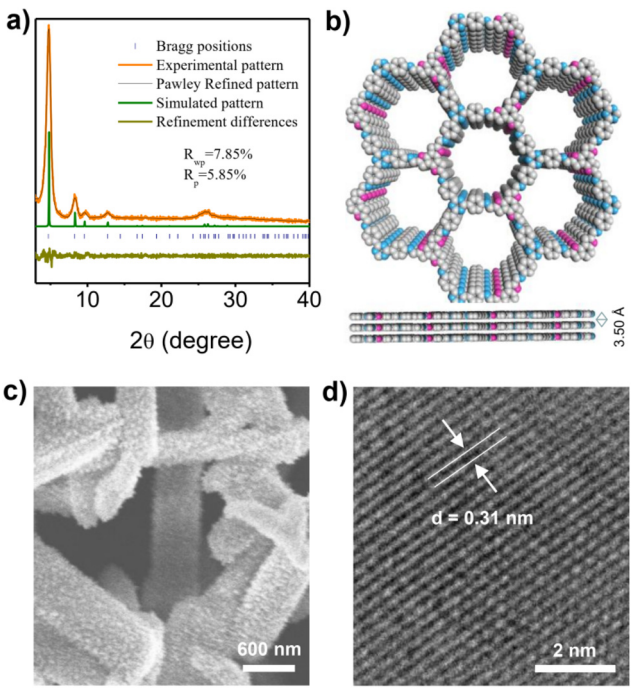

Fig. 4 (a) Experimental and simulated powder X-ray diffraction patterns of COF-JLU42. (b) Top and side views of the AA stacking structure of COF-JLU42 (gray, C; light blue, N; pink, O; H atoms are omitted). (c) FE-SEM image of COF-JLU42. (d) HR-TEM image of COF-JLU42.

tron microscopy (FE-TEM) images indicated that the COF-JLU42 is a pure solid phase with ribbon morphology (Fig. 4c). High-resolution transmission electron microscopy (HR-TEM) of COF-JLU42 displayed long-range ordered channels, further illustrating its high crystallinity (Fig. 4d and S2†). The lattice stripe spacing in the measured TEM photographs essentially matches the layer spacing of the AA stacking, which corresponds to the (001) crystal surface.

The thermal durability of COF-JLU42 was estimated *via* thermogravimetric analysis (TGA), which demonstrated a high thermal decomposition temperature of up to 520 °C under an N_2 atmosphere (Fig. S3†). Additionally, we also researched the chemical stability and photochemical durability of the new COF material. The COF-JLU42 sample was treated with methanol (MeOH), tetrahydrofuran (THF), H_2O, HCl (6 M), and NaOH (6 M) aqueous solution for 72 h at room temperature. Then samples were collected by centrifugation, washed, and dried in a vacuum. Pleasantly, all obtained samples maintained high crystallinity and skeleton connection as demonstrated by PXRD and FT-IR spectra (Fig. S4†), ever under irradiation with an OLED lamp. The results of the control experiment indicated the excellent durability of COF-JLU42.

The ultraviolet-visible diffuse reflectance (UV-vis DR) spectrum of COF-JLU42 showed a wide visible-light harvesting extending into 800 nm with maximum peaks at 439 nm (Fig. 5a), which is consistent with its color (Fig. 5a, inset). Based on the absorption band using the Tauc plot analysis, the optical band gap energy (E_g) was calculated to be 2.49 eV. Furthermore, the Mott–Schottky measurements were conducted and we evaluated the conduction band minimum (CBM) of COF-JLU42 to be −1.01 V *vs.* SCE (Fig. 5b). Therefore, the valence band maximum (VBM) can be estimated to be 1.48 V (*vs.* SCE) for COF-JLU42 according to the equation $E_g = E_{VB} - E_{CB}$, and the band structure alignment is displayed in Fig. S5d.† Furthermore, the density functional theory (DFT) calculations were still performed for both COF-JLUs. Their projected density of states (PDOS) and the band structures are presented in Fig. 5d and S6a.† We found that the CB mainly originated from TAPT and VB came from BTF-TC for COF-JLU42 or BTT-TC for COF-JLU32, which is consistent with the molecular orbital contributions, as displayed in Fig. 5e and S6b,† where the lowest unoccupied molecular orbital (LUMO) and the highest occupied molecular orbital (HOMO) mainly resulted from the acceptor TAPT and the donor BTF-TC or BTT-TC, respectively. These findings indicated that the two isomorphic COF-JLUs have similar absorption, E_g, and energy levels, which meet the thermodynamical requirement of photocatalytic proton reduction.

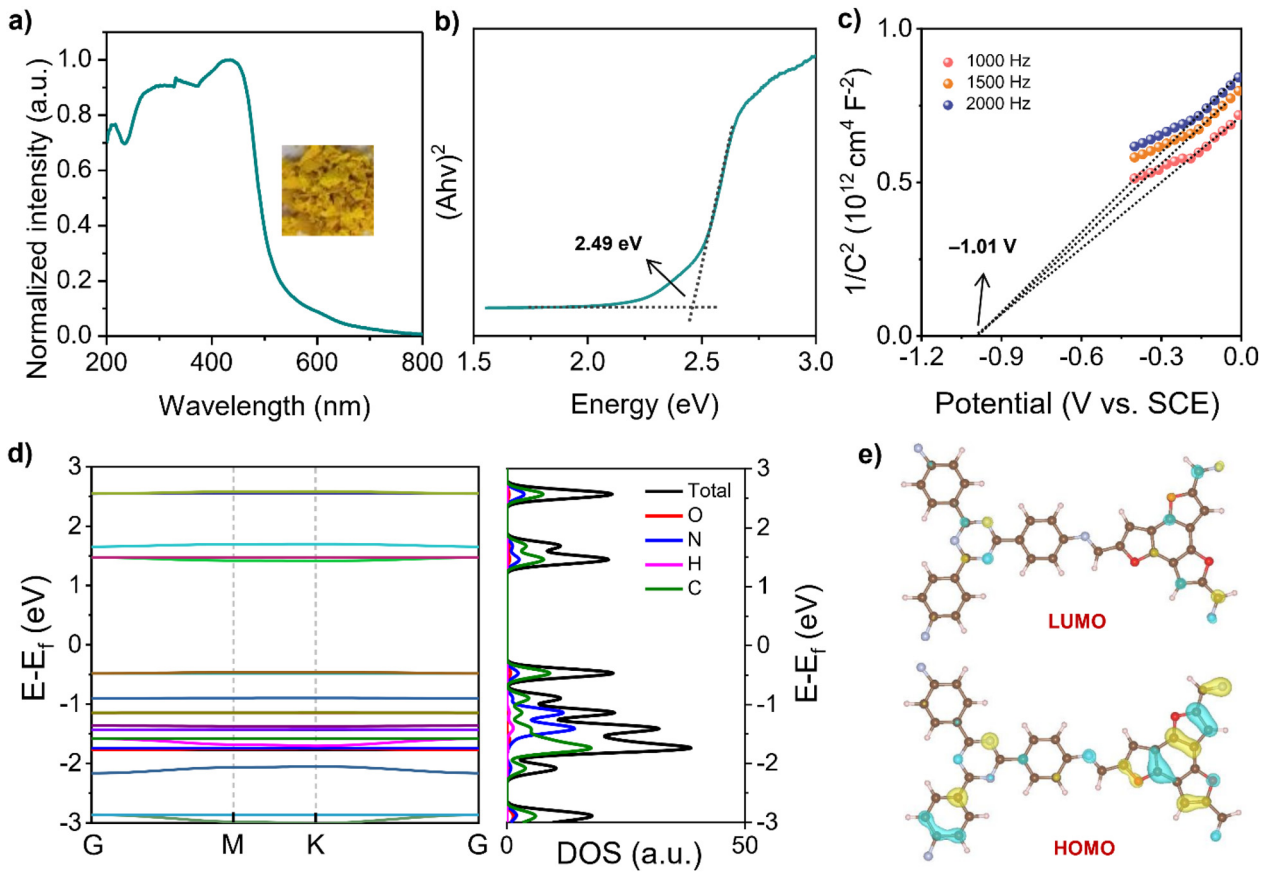

Fig. 5 (a) UV–vis DRS spectrum of COF-JLU42; inset: its photograph. (b) Tauc plots of COF-JLU42. (c) Mott–Schottky plots of COF-JLU42. (d) Calculated band structure and the density of states for COF-JLU42. (e) Kohn–Sham orbitals of LUMO and HOMO of COF-JLU42 (yellow: the positive phase of the molecular orbital wave function, blue: the negative phase of the molecular orbital wave function).

Subsequently, the photocatalytic hydrogen generation of COF-JLU42 *via* water splitting was explored to evaluate the inherent photoactivity of benzotrifuran-based framework materials. For the COF-JLU42-based photocatalytic system, ascorbic acid (AA) and platinum (Pt) nanoparticles were employed as the sacrificial electron donor (SED) and co-catalyst to facilitate hydrogen evolution.[22,23] The results of the control experiment showed that the photo-deposited Pt content seriously affected the hydrogen production rate of the framework (Fig. S7†). For instance, 5 mg of COF sample with 3 wt% Pt was dispersed in 50 mL of an aqueous solution and displayed an average hydrogen evolution rate (HER) of 17 790 μmol g^{-1} h^{-1} under visible-light illumination (420 < λ < 780 nm), which is higher than that of isomorphic COF-JLU32 (10 710 μmol g^{-1} h^{-1}) under the same conditions (Fig. 6a). The average HER of COF-JLU42 improved to 28 650 μmol g^{-1} h^{-1} and 3 mg of the polymer with 3 wt% Pt was utilized (Fig. S8†). Furthermore, reducing the mass of COF to 1 mg, surprisingly, a superior HER of 40 430 μmol g^{-1} h^{-1} was obtained (Fig. S7†), which exceeded that of the state-of-the-art COF-based photocatalysts (Table S2†). In sharp contrast, the photocatalytic activity of COF-JLU32 (16 080 μmol g^{-1} h^{-1}) was less than half that of COF-JLU42 under the same conditions, although the former had a larger surface area (Fig. S9) and higher crystallinity (Fig. S1†).

Furthermore, the apparent quantum yield (AQY) of COF-JLU42 and COF-JLU32 were also conducted under monochromatic incident light. As depicted in Fig. S10a,† the highest AQY of 1.18% at 450 nm for COF-JLU42 was obtained, which surpassed those of the well-known photocatalysts such as N_3-COF ($AQY_{450\ nm}$ = 0.44%),[47] sp^2c-COF_{ERDN} ($AQY_{490\ nm}$ = 0.48%),[46] and g-$C_{40}N_3$-COF ($AQY_{420\ nm}$ = 1.10%).[40] Moreover, the AQYs were estimated to be 0.85%, 0.47%, and 0.26% at 420, 500, and 550 nm, respectively. In addition, the AQY of COF-JLU32 also showed a similar wavelength-dependent trend, with the highest value of 0.63% at 450 nm, which is smaller than that of the isomorphic COF-JLU42 (Fig. S10b†). Next, the stability of both COF-JLUs as photocatalysts for hydrogen evolution *via* water splitting was evaluated by repeated experiments. No significant loss of photocatalytic activity was obtained during the measurement period, even after five cycles of at least 20 h, and the FT-IR, PXRD, UV-Vis spectrum, surface area, and FE-SEM data were comparable with those of the original COF samples (Fig. S11†).

In order to study the difference in the photocatalytic activity of the two isomorphic COFs for hydrogen evolution, a series of photoelectric experiments were performed. It is well known that the highly efficient generation, separation, and transport of the photogenerated charge carriers in the semiconductor photocatalyst are crucial for improving photocatalytic activity.

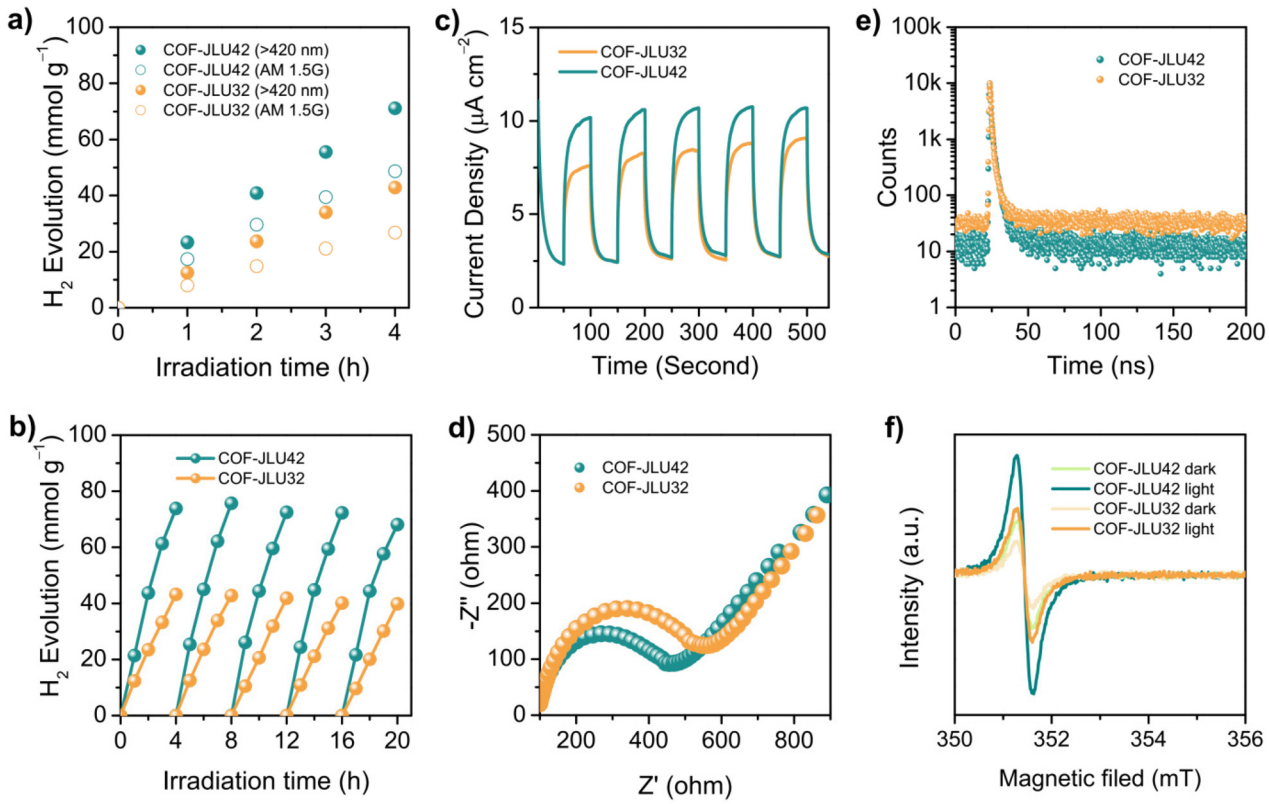

Fig. 6 (a) Photocatalytic hydrogen evolution activity of COF-JLUs under visible-light irradiation (λ > 420 nm) and AM 1.5G (5 mg of COF-JLU in 50 mL of H_2O, 3 wt% Pt as a cocatalyst, 0.1 M AA as SED). (b) Photocatalytic stability of COF-JLUs (5 mg of COF-JLU in 50 mL of H_2O, 3 wt% Pt as a cocatalyst, 0.1 M AA as SED, λ > 420 nm). (c) Transition photocurrents of COF-JLUs under visible-light illumination. (d) EIS spectra of COF-JLUs. (e) Time-resolved PL spectra of COF-JLUs. (f) EPR conduction band electron spectra of COF-JLUs in the dark and under visible-light illumination.

Accordingly, transient photocurrent response and electrochemical impedance spectroscopy (EIS) were first conducted. Under light illumination, two materials exhibited fast photocurrent responses with a few reduplicative cycles of intermittent on–off irradiation, which provided clear evidence for the photogenerated carrier transport (Fig. 6c). Obviously, COF-JLU42 showed a stronger transient photocurrent than that of COF-JLU32, suggesting the more convenient dissociation of photoinduced electron/hole pairs. As shown in Fig. 6d, furthermore, the EIS Nyquist plots exhibited that the semicircle diameter of COF-JLU42 is smaller than that of COF-JLU32, indicating more effectively photogenerated charge carrier transport and separation in COF-JLU42, thus restricting the electron–hole recombination more effectively.[48,49] In addition, time-resolved fluorescence decay spectroscopy of COF-JLUs was recorded. As displayed in Fig. 6e, the average lifetime was calculated to be 1.85 ns for COF-JLU42 and 1.62 ns for COF-JLU32, respectively. The longer lifetime of COF-JLU42 implies stronger separation of the charge carriers compared with that of COF-JLU32, which also corresponds to better photocatalytic activity. Then, electron spin-spectroscopy was carried out to further explore the charge separation efficiency of the two COFs. As shown in Fig. 6f, both COF-JLUs represented an isotropic peak with a Lorentzian-type pattern at g = 2.003 under light illumination and dark, which follows the electrons in the π-delocalized aromatic frameworks.[50] COF-JLU42 revealed a much stronger signal intensity than the isomorphic COF-JLU32 in the dark or under light irradiation, suggesting a large charge separation efficiency of COF-JLU42.

We further investigated the temperature-dependent photoluminescence (PL) spectra to evaluate the exciton dynamics properties. As shown in Fig. 7 insets, the PL intensity of both COF-JLUs increased monotonically as the temperature decreased, indicating the thermal quenching phenomenon of PL emission in the research temperature scope.[45,51–54] By fitting the temperature dependence of the integrated PL intensities as a function of temperature according to the Arrhenius equation: $I(T) = I_0/[1 + A\exp(-E_b/k_BT)]$ (where I_0 is the intensity at 0 K, T is the temperature, and k_B is the Boltzmann constant), the E_b of both COFs can be obtained. As displayed in Fig. 7, the E_b values for COF-JLU42 and COF-JLU32 were calculated to be 81.7 and 128.5 meV, respectively. The smaller E_b value indicates that the charge separation is more likely to occur in COF-JLU42. All these observations provided the structural advantages of a benzotrifuran-based donor–acceptor framework for improving photocatalytic activity.

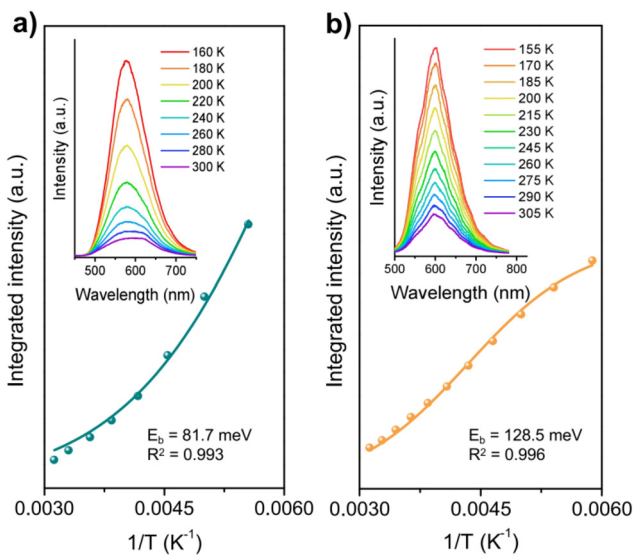

Fig. 7 Integrated PL emission intensity as a function of the temperature of COF-JLU42 (a) and COF-JLU32 (b), respectively. Inset: the corresponding temperature-dependent PL spectra.

Conclusions

In summary, a novel benzotrifuran-based covalent organic framework (COF-JLU42) was successfully designed and constructed *via* the imine condensation reaction under solvothermal conditions. Experimental and theoretical studies indicated that the new COF material had strong crystallinity, a high surface area, superior durability, and good photoelectric properties with small exciton binding energy. More significantly, the benzotrifuran-based COF exhibited a high hydrogen evolution rate of up to 40 430 μmol g^{-1} h^{-1} under visible-light illumination with outstanding reusability, which is higher than the isomorphic benzotrithiophene-based COF (COF-JLU32). We believe that this work will open up a new avenue for the preparation of benzotrifuran-based porous functional materials at the molecular level. Currently, such studies are underway in our laboratory.

Author contributions

X. L. conceived the project, designed experiments, and provided funding. C. Y. and Z. Z. conducted the experiments and analyzed the data. Q. Z. performed the theoretical data calculations and analyzed the results. J. L., Y. H., H. Y., and Z. L. provided experimental testing support and gave useful help during the experiments. X. L. and C. Y. wrote the manuscript and discussed the results with all authors.

Conflicts of interest

The authors declare no competing financial interest.

Acknowledgements

This work was supported by the project of the National Natural Science Foundation of China (No. 52073119, 52373210), Natural Science Foundation of Jilin Province (No. 20230101029JC), and State Key Laboratory of Inorganic Synthesis and Preparative Chemistry (No. 2024-7).

References

1 Y. Wang, A. Vogel, M. Sachs, R. S. Sprick, L. Wilbraham, S. J. A. Moniz, R. Godin, M. A. Zwijnenburg, J. R. Durrant, A. I. Cooper and J. Tang, *Nat. Energy*, 2019, **4**, 746–760.

2 B. Shao, Z. Liu, L. Tang, Y. Liu, Q. Liang, T. Wu, Y. Pan, X. Zhang, X. Tan and J. Yu, *J. Hazard. Mater.*, 2022, **435**, 129067.

3 B. Shao, L. Shen, Z. Liu, L. Tang, X. Tan, D. Wang, W. Zeng, T. Wu, Y. Pan, X. Zhang, L. Ge and M. He, *Chem. Eng. J.*, 2023, **455**, 140476.

4 Z. Liu, M. He, L. Tang, B. Shao, Q. Liang, T. Wu, Y. Pan, X. Zhang, S. Luo, Q. He and L. Ge, *J. Colloid Interface Sci.*, 2023, **634**, 255–267.

5 T. Banerjee, F. Podjaski, J. Kröger, B. P. Biswal and B. V. Lotsch, *Nat. Rev. Mater.*, 2020, **6**, 168–190.

6 J. Schneider, M. Matsuoka, M. Takeuchi, J. Zhang, Y. Horiuchi, M. Anpo and D. W. Bahnemann, *Chem. Rev.*, 2014, **114**, 9919–9986.

7 T. Takata, J. Jiang, Y. Sakata, M. Nakabayashi, N. Shibata, V. Nandal, K. Seki, T. Hisatomi and K. Domen, *Nature*, 2020, **581**, 411–414.

8 X. Wang, K. Maeda, A. Thomas, K. Takanabe, G. Xin, J. M. Carlsson, K. Domen and M. Antonietti, *Nat. Mater.*, 2009, **8**, 76–80.

9 W. Ting, Z. F. Liu, B. B. Shao, Q. H. Liang, Q. Y. He, P. Yuan, X. S. Zhang, Y. Liu, J. W. Sun and S. X. Gong, *Chem. Eng. J.*, 2022, **447**, 137332.

10 T. Wu, Q. Liang, L. Tang, J. Tang, J. Wang, B. Shao, S. Gong, Q. He, Y. Pan and Z. Liu, *J. Hazard. Mater.*, 2023, **443**, 130251.

11 Y. Pan, Z. Peng, Z. Liu, B. Shao, Q. Liang, Q. He, T. Wu, X. Zhang, C. Zhao, Y. Liu, L. Ge and M. He, *J. Environ. Chem. Eng.*, 2022, **10**, 107366.

12 T. Wu, Q. He, Z. Liu, B. Shao, Q. Liang, Y. Pan, J. Huang, Z. Peng, Y. Liu, C. Zhao, X. Yuan, L. Tang and S. Gong, *J. Hazard. Mater.*, 2022, **424**, 127177.

13 X. Zhang, S. Tong, D. Huang, Z. Liu, B. Shao, Q. Liang, T. Wu, Y. Pan, J. Huang, Y. Liu, M. Cheng and M. Chen, *Coord. Chem. Rev.*, 2021, **448**, 214177.

14 P. J. Waller, F. Gándara and O. M. Yaghi, *Acc. Chem. Res.*, 2015, **48**, 3053–3063.

15 K. Geng, T. He, R. Liu, S. Dalapati, K. T. Tan, Z. Li, S. Tao, Y. Gong, Q. Jiang and D. Jiang, *Chem. Rev.*, 2020, **120**, 8814–8933.

16 Y. Song, Q. Sun, B. Aguila and S. Ma, *Adv. Sci.*, 2018, **6**, 1801410.

17 S. Y. Ding and W. Wang, *Chem. Soc. Rev.*, 2013, **42**, 548–568.

18 T. Li, Y. Pan, B. Shao, X. Zhang, T. Wu, Q. He, M. He, L. Ge, L. Zhou, S. Liu, X. Zheng, J. Ye and Z. Liu, *Adv. Funct. Mater.*, 2023, **33**, 2304990.

19 R. Liu, K. T. Tan, Y. Gong, Y. Chen, Z. Li, S. Xie, T. He, Z. Lu, H. Yang and D. Jiang, *Chem. Soc. Rev.*, 2021, **50**, 120–242.

20 T. He and Y. Zhao, *Angew. Chem., Int. Ed.*, 2023, **62**, e202303086.

21 H. Chen, H. S. Jena, X. Feng, K. Leus and P. V. D. Voort, *Angew. Chem., Int. Ed.*, 2022, **61**, e202204938.

22 Z. Li, J. Wang, S. Ma, Z. Zhang, Y. Zhi, F. Zhang, H. Xia, G. Henkeim and X. Liu, *Appl. Catal., B*, 2022, **310**, 121335.

23 Z. Zhang, J. Jia, Y. Zhi, S. Ma and X. Liu, *Chem. Soc. Rev.*, 2022, **51**, 2444–2490.

24 Z. Li, T. Deng, S. Ma, Z. Zhang, G. Wu, J. Wang, Q. Li, H. Xia, S. Yang and X. Liu, *J. Am. Chem. Soc.*, 2023, **145**, 8364–8374.

25 S. Ma, T. Deng, Z. Li, Z. Zhang, J. Jia, G. Wu, H. Xia, S. Yang and X. Liu, *Angew. Chem., Int. Ed.*, 2022, **61**, e202208919.

26 L. Stegbauer, K. Schwinghammer and B. V. Lotsch, *Chem. Sci.*, 2014, **5**, 2789–2793.

27 X. Wang, L. Chen, S. Y. Chong, M. A. Little, Y. Wu, W.-H. Zhu, R. Clowes, Y. Yan, M. A. Zwijnenburg, R. S. Sprick and A. I. Cooper, *Nat. Chem.*, 2018, **10**, 1180–1189.

28 J. Yang, A. Acharjya, M. Y. Ye, J. Rabeah, S. Li, Z. Kochovski, S. Youk, J. Roeser, J. Grüneberg, C. Penschke, M. Schwarze, T. Wang, Y. Lu, R. Krol, M. Oschatz, R. Schomäcker, P. Saalfrank and A. Thomas, *Angew. Chem., Int. Ed.*, 2021, **60**, 19797–19803.

29 R. Chen, Y. Wang, Y. Ma, A. Mal, X. Y. Gao, L. Gao, L. Qiao, X. B. Li, L. Z. Wu and C. Wang, *Nat. Commun.*, 2021, **12**, 1354.

30 Y. Li, L. Yang, H. He, L. Sun, H. Wang, X. Fang, Y. Zhao, D. Zheng, Y. Qi, Z. Li and W. Deng, *Nat. Commun.*, 2022, **13**, 1355.

31 S. Wei, F. Zhang, W. Zhang, P. Qiang, K. Yu, X. Fu, D. Wu, S. Bi and F. Zhang, *J. Am. Chem. Soc.*, 2019, **141**, 14272–14279.

32 Y. Wang, W. Hao, H. Liu, R. Chen, Q. Pan, Z. Li and Y. Zhao, *Nat. Commun.*, 2022, **13**, 100.

33 W. Dong, Z. Qin, K. Wang, Y. Xiao, X. Liu, S. Ren and L. Li, *Angew. Chem., Int. Ed.*, 2023, **62**, e2022160.

34 S. Li, R. Ma, S. Xu, T. Zheng, G. Fu, Y. Wu, Z. Liao, Y. Kuang, Y. Hou, D. Wang, P. S. Petkov, K. Simeonova, X. Feng, L. Wu, X. Li and T. Zhang, *J. Am. Chem. Soc.*, 2022, **144**, 13953–13960.

35 S. Ghosh, A. Nakada, M. A. Springer, T. Kawaguchi, K. Suzuki, H. Kaji, I. Baburin, A. Kuc, T. Heine, H. Suzuki, R. Abe and S. Seki, *J. Am. Chem. Soc.*, 2020, **142**, 9752–9762.

36 W. Chen, L. Wang, D. Mo, F. He, Z. Wen, X. Wu, H. Xu and L. Chen, *Angew. Chem., Int. Ed.*, 2020, **59**, 16902–16909.

37 S. Zhang, G. Cheng, L. Guo, N. Wang, B. Tan and S. Jin, *Angew. Chem., Int. Ed.*, 2020, **59**, 6007–6014.

38 M. Liu, Q. Huang, S. Wang, Z. Li, B. Li, S. Jin and B. Tan, *Angew. Chem., Int. Ed.*, 2018, **57**, 11968–11972.

39 Z. Xie, X. Yang, P. Zhang, X. Ke, X. Yuan, L. Zhai, W. Wang, N. Qin, H. Cui, L. Qu and X. Chen, *J. Chin. Catal.*, 2023, **47**, 171–180.

40 C. Li, J. Liu, H. Li, K. Wu, J. Wang and Q. Yang, *Nat. Commun.*, 2022, **13**, 2357.

41 W. Weng and J. Guo, *Nat. Commun.*, 2022, **13**, 5768.
42 H. Tsuji, C. Mitsui, L. Ilies, Y. Sato and E. Nakamura, *J. Am. Chem. Soc.*, 2007, **129**, 11902–11903.
43 Z. Li, H. Li, S. Chen, T. Froehlich, C. Yi, C. Schönenberger, M. Calame, S. Decurtins, S. Liu and E. Borguet, *J. Am. Chem. Soc.*, 2014, **136**, 8867–8870.
44 W. An, S. Zheng, X. Xu, L. Liu, J. Ren, L. Fan, Z. Yang, Y. Ren and C. Xu, *Appl. Catal., B*, 2022, **316**, 121630.
45 G. Wang, F. Zhu, Q. Lin, J. Kan, K. Xie, S. Li, Y. Geng and Y. Dong, *Chem. Commun.*, 2021, **57**, 4464–4467.
46 J. Li, Z. Zhang, J. Jia and X. Liu, *Chem. Res. Chin. Univ.*, 2022, **38**, 275–289.
47 V. S. Vyas, F. Haase, L. Stegbaur, G. Savasci, F. Podjaski, C. Ochsenfeld and B. V. Lotsch, *Nat. Commun.*, 2015, **6**, 8508.
48 E. Jin, Z. Lan, Q. Jiang, K. Geng, G. Li, X. Wang and D. Jiang, *Chem*, 2019, **5**, 1632–1647.
49 S. Bi, C. Yang, W. Zhang, J. Xu, L. Liu, D. Wu, X. Wang, Y. Han, Q. Liang and F. Zhang, *Nat. Commun.*, 2019, **10**, 2467.
50 H. Liu, X. Zheng, J. Xu, X. Jia, M. Chao, D. Wang and Y. Zhao, *ACS Appl. Mater. Interfaces*, 2023, **15**, 16794–16800.
51 K. Huang, J. Bai, R. Shen, X. Li, C. Qin, P. Zhang and X. Li, *Adv. Funct. Mater.*, 2023, 2307300.
52 Z. Lan, M. Wu, Z. Fang, Y. Zhang, X. Chen, G. Zhang and X. Wang, *Angew. Chem., Int. Ed.*, 2022, **61**, e202201482.
53 Z. Xie, X. Yang, P. Zhang, X. Ke, X. Yuan, L. Zhai, W. Wang, N. Qin, C. Cui, L. Qu and X. Chen, *Chin. J. Catal.*, 2023, **47**, 171–180.
54 S. Chai, X. Chen, X. Zhang, Y. Fang, R. S. Sprick and X. Chen, *Environ. Sci.: Nano*, 2022, **9**, 2464–2469.